

Article

Microstructural and Mechanical Properties of Cement Blended with TEOS/PVP Nanofibers Containing CNTs

Tri N. M. Nguyen ¹, Taek Hee Han ², Jun Kil Park ² and Jung J. Kim ^{3,*}

¹ Campus in Ho Chi Minh City, University of Transport and Communications, No. 450-451 Le Van Viet Street, Tang Nhon Phu A Ward, Thu Duc City, Ho Chi Minh City 700000, Vietnam

² Coastal Development and Ocean Energy Research Center, Korea Institute of Ocean Science and Technology, 385 Haeyang-ro, Yeongdo-gu, Busan 49111, Republic of Korea

³ Department of Civil Engineering, Kyungnam University, 7 Kyungnamdaehakro, Changwon-si 51767, Republic of Korea

* Correspondence: jungkim@kyungnam.ac.kr; Tel.: +82-55-249-6421; Fax: +82-505-999-2165

Abstract: In this investigation, we mixed cement with electrospun nanofibers made of tetraethoxysilane (TEOS) and polyvidone (PVP), as well as a modified version with carbon nanotubes (CNT). When we incorporated TEOS/PVP and CNT-TEOS/PVP nanofibers into the cementitious materials, the results of mechanical strength tests showed improvements in compressive strength of 28% and 38% and in toughness of 54% and 66%, respectively. We observed the morphology and texture of the fibers using a scanning electron microscope (SEM) and transmission electron microscope (TEM) analyses. In addition, based on our SEM, energy-dispersive spectroscopy (EDS), and thermogravimetric analysis (TGA), we observed that the matrix structure was compacted due to the nanofiber's matrix-bridging effect and the increase in hydration products. Therefore, the results of our microstructure studies agree with those of the mechanical strength tests. Our findings can be used to increase cement quality while lowering overall usage, thereby minimizing its environmental impacts.

Keywords: TEOS; PVP; CNT; cement; electrospun nanofibers; microstructure; compressive strength; toughness



Citation: Nguyen, T.N.M.; Han, T.H.; Park, J.K.; Kim, J.J. Microstructural and Mechanical Properties of Cement Blended with TEOS/PVP Nanofibers Containing CNTs. *Appl. Sci.* **2023**, *13*, 714. <https://doi.org/10.3390/app13020714>

Academic Editor: Bing Chen

Received: 10 December 2022

Revised: 30 December 2022

Accepted: 3 January 2023

Published: 4 January 2023



Copyright: © 2023 by the authors. Licensee MDPI, Basel, Switzerland. This article is an open access article distributed under the terms and conditions of the Creative Commons Attribution (CC BY) license (<https://creativecommons.org/licenses/by/4.0/>).

1. Introduction

The cement industry is one of the most non-ecological and creates huge emissions. Therefore, exploring ways to make the cement industry environmentally friendly is of considerable worldwide concern. Hamada et al. [1] used a response surface methodology to demonstrate the efficiency of palm oil clinker and nano-palm-oil fuel ash in the production of concrete and helped to achieve environmental sustainability by lowering the production of agricultural and industrial waste byproducts. Further studies have improved cement matrix characteristics to reduce cement usage. Recently, nanoscale materials have caught the interest of researchers and are commonly used in cement-based products. According to Zhang et al., cement-based materials containing nano-silica and superabsorbent polymer can be used in practical engineering thanks to their low shrinkage and high ductility characteristics [2]. Wang et al. [3,4] pointed out the effect of carbon nanofibers on improving the electrical resistivity and capacitive reactance of cement pastes, and they observed that the highest self-sensing performance sensitivity corresponded to a carbon nanofiber dosage of 2.5%. Saleh et al. [5,6] showed the effectiveness of titanate nanofibers in modifying cementitious materials to produce anti-radioactive or hazardous waste containers. We conducted a literature review and found that researchers were most concerned with the mechanical characteristics of nanofibers-modified cementitious materials. Many types of nanofibers were applied to cement in different directions to analyze its mechanical behavior. For instance, Chinchillas-Chinchillas et al. [7] reported increases in compressive and flexural strength of 26.1% and 89.1%, respectively, and a decline of 93.1% in the drying

shrinkage of cement mortar containing recycled PET/PAN nanofibers. McElroy et al. [8] enhanced the compressive and tensile strength of oil-well cement up to 50% and 53%, respectively, by adding alumina nanofibers to the paste. Azevedo and Gleize [9] reported an increase of 74.77% and 24.87% in flexural and compressive strength, respectively, after adding different dosages of silicon carbide nanofibers into Portland cement pastes. Al-Rub et al. [10] observed increases in ductility, flexural strength, Young's modulus, and toughness of 73%, 60%, 25%, and 170% on average, respectively, after adding carbon nanofibers or carbon nanotubes into cement pastes. In almost all of the above cases, nanofibers were incorporated into cementitious materials by first dispersing in water to form an aqueous solution and then mixing the as-solution with cement powder. The dispersion of the precursors in water is a complicated process, normally conducted with the help of ultrasonic energy [8,9] or the addition of surfactant agents (i.e., superplasticizers) into the mix [3,4,9,10]. From another perspective, the previous works [11–13] presented another approach to combine electrospun nanofibers with cement powder. Nanofibers were fabricated and blended with cement powder through the electrospinning process using an improved collector.

Electrospinning is a flexible and economical technology for creating nanofibers made of various materials that are appropriate for a variety of applications [14–16]. The general principle of the electrospinning technique is based on the electrostatic repulsion between the strongly charged polymer solutions and the negative collector, which fabricates nano-sized fibers. Our literature review showed that tetraethoxysilane/polyvidone nanofibers (TEOS/PVP NFs) fabricated by the electrospinning technique were utilized in numerous fields, such as catalytic applications [17], protein detection [18], wound-dressing applications [19], drug-delivery systems [20], etc. However, the literature rarely explored its application in enhancing cement matrix strength. Therefore, the goal of our study is to investigate the changes in the mechanical and microstructural properties of ordinary Portland cement (OPC) blended with TEOS/PVP NFs, as well as versions modified by carbon nanotubes (CNT-TEOS/PVP NFs). To the best of our knowledge, silica is TEOS/PVP's primary ingredient. Where PVP is a carrier matrix and TEOS is a precursor to silica [21]. Therefore, it is anticipated that adding TEOS/PVP NFs to cement will result in more pozzolanic reactions. These nanofibers can, therefore, efficiently raise the amount of hydration products in the matrix, enhancing its mechanical characteristics and toughness. According to the findings of earlier research [11], CNTs have demonstrated their value in enhancing the tensile strength of cement paste when combined with nylon 66 nanofibers. To continue this strategy, CNTs have been introduced to TEOS/PVP NFs to examine their impact on the pastes' tensile strength. Positive results regarding the mechanical properties of cement can be considered as a premise for improving the quality of this material, reducing the amount of cement used and thereby minimizing its environmental impacts. The nanofibers were fabricated by the electrospinning process [17,18,22–25] and blended directly into cement powder [11,12]. In our study, we modified TEOS/PVP NFs using multi-walled carbon nanotubes (MWCNTs), and we conducted the ultrasonication process while preparing the polymer solution to break the strong van der Waals forces that cause the agglomeration of carbon nanotubes (CNTs) [26–29].

Above all, the primary goal of this study is to examine the mechanical and microstructural characteristics of cementitious materials blended with TEOS/PVP NFs and CNT-TEOS/PVP NFs. Our mechanical strength test results showed how our proposed electrospun nanofibers affected some key properties of cement. We also carried out microstructure analyses, such as the field emission transmission electron microscope (FE-TEM) and the field emission scanning electron microscope (FE-SEM), to confirm the changes in the nanofibers' morphology as well as the matrix's microstructure. Furthermore, we performed energy-dispersive spectroscopy (EDS) and thermogravimetric analysis (TGA) to examine the variation in hydration-product proportions.

2. Experiments

2.1. Materials

We utilized type I OPC cement from Ssangyong Co, Korea, in compliance with ASTM C150 [30]. Table 1 presents the chemical components and physical characteristics of OPC.

Table 1. Chemical composition and physical characteristics of OPC.

CaO	61.33
SiO ₂	21.01
Al ₂ O ₃	6.40
SO ₃	2.30
MgO	3.02
Fe ₂ O ₃	3.12
Ig. loss	1.40
Compressive strength at 28 days (MPa)	36
Specific surface area (cm ² /g)	2800

We used TEOS (Tetraethoxysilane; Cas No 78-10-4; Alfa Aesar, Germany), PVP (polyvi-done; Cas No 9003-39-8; Sigma-Aldrich, USA), butanol (Cas No 71-36-3; Sigma-Aldrich, USA), and MWCNTs (multi-walled carbon nanotubes; diameter: 10 nm, length: 30 μm; grade: CM-95; Hanos, Republic of Korea) to prepare the polymer solution. We employed all chemicals as received. Table 2 presents the properties of the chemicals.

Table 2. Properties of TEOS, PVP, and butanol.

Properties	TEOS	PVP	Butanol
Linear formula	(C ₂ H ₅ O) ₄ Si	(C ₆ H ₉ NO) _n	C ₄ H ₁₀ O
Molecular weight (g/mol)	208.329	1,300,000	74.12
Purity (%)	98	98	99.9
Density at 25 °C (g/mL)	0.934	1.2	0.81

2.2. Polymer Solution

The following steps present our polymer solutions preparation process: (1) Stirring TEOS and butanol with a volume proportion of 5:3 (TEOS: butanol) at 80 °C and 30 min; (2) adding and stirring PVP in the as-solution with a weight proportion of 1:9 (PVP: as-solution) at 120 °C and 90 min [25]. We added CNTs into the solution containing TEOS and butanol first to prepare the polymer solution containing CNTs and TEOS/PVP, in which the content of PVP was partly replaced by CNTs. Hence, the weight proportion between PVP and CNTs was 24:1. The literature shows that agglomerate phenomenon is normally due to the strong van der Waals links between CNT molecules [31–33]. Hence, we conducted the ultrasonication process during this period to obtain the homogeneous solution [26–29]. After finishing the preparation process, we kept the obtained polymer solutions for 24 h under laboratory conditions due to the relaxation of the polymer chain. Table 3 presents a summary of the polymer solution's component proportions.

Table 3. Components proportion of polymer solution by weight percent (%).

	Solvent	PVP	CNTs
TEOS/PVP polymer solution	90	10	-
CNT-TEOS/PVP polymer solution	90	9.6	0.4

2.3. Electrospinning Process

In our study, we fabricated TEOS/PVP NFs and CNT-TEOS/PVP NFs using an electrospinning system. We conducted the electrospinning processes similar to the process in [11,12] (see Figure 1). Information on the electrospinning process can be found in Table 4.

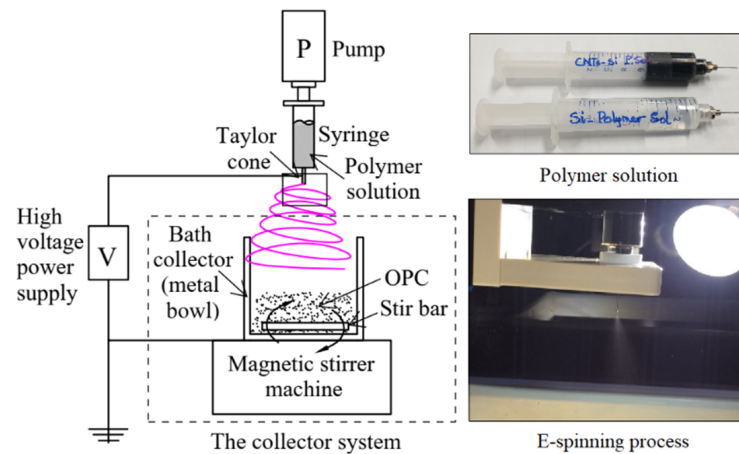


Figure 1. Electrospinning process and polymer solutions.

To analyze the morphological properties of TEOS/PVP NFs and CNT-TEOS/PVP NFs, we prepared the samples for FE-SEM and FE-TEM by electrospinning the nanofibers directly onto 5 mm × 5 mm carbon tapes and copper grids.

Table 4. Input parameter of the electrospinning process.

Voltage (kV)	12
Syringe (mL)	12
Needle	20
Working distance (mm)	60
Pump speed ($\mu\text{L}/\text{min}$)	30

2.4. Hardened Cement Pastes Preparation

Based on the blend method proposed in the previous works, we electrospun TEOS/PVP NFs and CNT-TEOS/PVP onto an improved collector for blending the nanofibers and cement powder [11,12]. The improved collector's mechanism is based on the rotation of a magnetic stir bar inside a metal bowl. The wall of the bowl needs to be insulated to concentrate the nanofibers jet onto the bottom of the bowl. A magnetic stirrer machine under the metal bowl supplies the magnetic energy for rotating the stir bar. The metal bowl is connected to the ground and works as the negative electrode of the system (see Figure 1). We conducted the blending process for every 95 g of OPC and 5 g of the polymer solution. Studying the mechanical characteristics of cement is very difficult because of the changes in volume as well as the development of spontaneous cracking during the curing period; therefore, samples of hardened cement pastes usually have small dimensions. We prepared the samples for the tensile and compressive strength tests in accordance with the specifications of ASTM C307 [34] and ASTM C109 [35]. We prepared six dogbone and five cubic samples for each type of cementitious material, kept a constant water-binder ratio of 0.5, demolded after 24 h, and cured for 28 days in the water under 23 ± 2 °C with an RH higher than 50% (see Figure 2). The mix proportions of the cement-based materials are shown in Table 5.

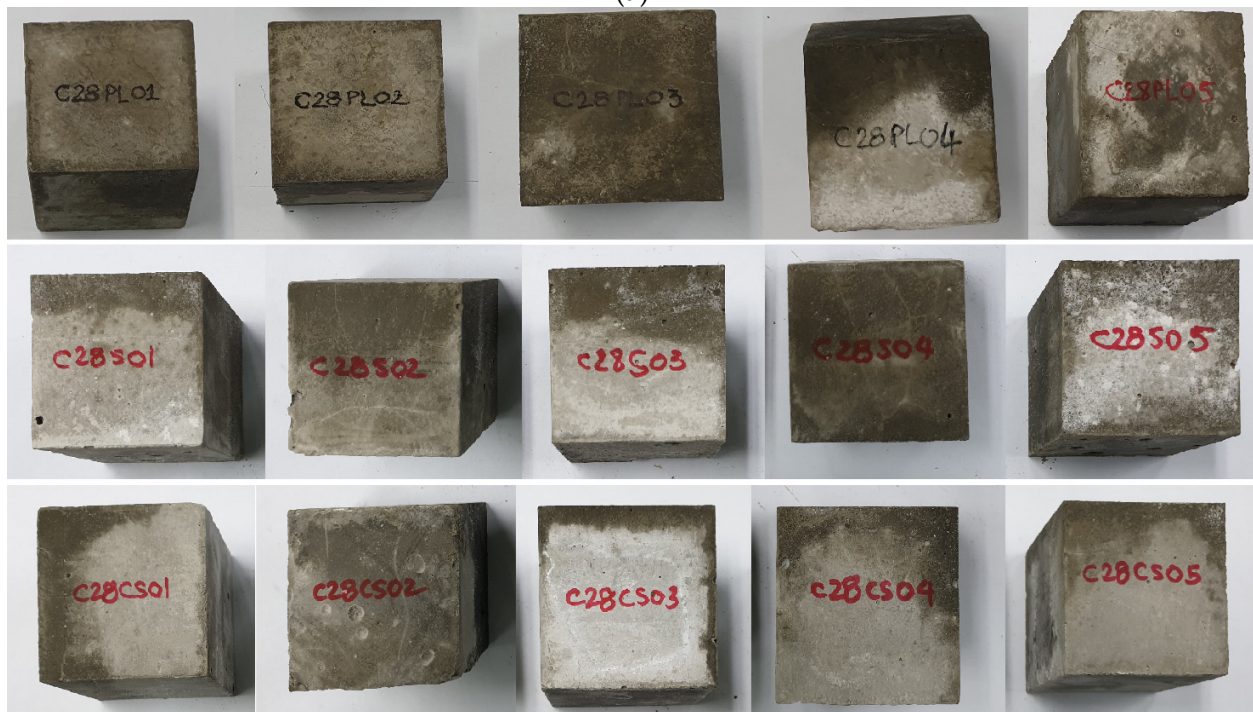
Table 5. Mix proportions of cement-based materials (by % mass).

Samples	Binder (B)			Water/B
	OPC	TEOS/PVP NFs	CNTs	
Plain paste	100	0	0	0.5
T28S/C28S	99.7	3.3	0	0.5
T28CS/C28CS	99.7	3.3	0.02	0.5

We utilized the broken samples gathered from the mechanical strength test for SEM analysis to analyze the cement matrix's microstructure. We prepared the 0.5 mm thick SEM samples. In addition, we also prepared micro-sized samples of each cementitious material for TGA.



(a)



(b)

Figure 2. Samples for tensile and compressive strength tests: (a) dogbone samples for tensile strength test; (b) cubic samples for compressive strength test (T: tension; C: compression; 28: curing time (days); PL: plain paste; S: TEOS/PVP NFs-blended cement paste; CS: CNT-TEOS/PVP NFs-blended cement paste).

2.5. Apparatus and Methodology

In our study, we performed the tensile strength tests according to ASTM C307 [34] using a mortar tensile strength test machine with a capacity of 5 kN. We used the hydraulic universal testing device with a capacity of 1000 kN for the compressive strength tests according to ASTM C109 [35]. We analyzed the morphology of the nanofibers, the microstructure of the cement matrix, and the local chemical components of the samples by FE-SEM and EDS analyses using the Zeiss Merlin Compact system. We set the input parameters as: working distance from 7.1 to 7.9 mm and accelerating voltage from 3 to 5 kV. We coated a 5Å-platinum layer on the sample surface to improve the image resolution. We performed FE-TEM using the FEI Tecnai F30 Twin system under an acceleration voltage of 300 kV. Finally, we conducted a thermogravimetric analysis using TA instrument SDT-Q600 and set the input parameters as: heating range: 25 °C–1000 °C, nitrogen atmosphere, heating velocity: 10 °C/min, flow rate: 100 mL/min.

3. Results and Discussion

3.1. Tensile and Compressive Strength

We investigated the influence of TEOS/PVP nanofibers, including those modified by carbon nanotubes, on the mechanical characteristics of hardened cement pastes using 28-day tensile and compressive strength tests. Figure 3 shows that the tensile strength of the nanofibers-blended cement pastes increased slightly by around 6% and 10% compared with that of the plain paste in comparisons between the tensile strength results of the T28S and T28CS samples, respectively, and the T28PL sample. These unimpressive results show the inefficiency of TEOS/PVP NFs and CNT-TEOS/PVP NFs in increasing the tensile strength of the cement pastes. Previous studies have clarified the increase in tensile strength of the pastes when blending nylon 66 nanofibers and their modified versions with cement using the same method [11,12]. The comparison results are shown in Table 6. In contrast, there was a significant increase in compressive behaviors when modifying cement with the proposed fibers compared with those of plain paste (see Figures 4 and 5 and Table 7). The results show an increase of 28% and 38% in compressive strength and 54% and 66% in toughness when comparing the C28S and C28CS samples, respectively, with C28PL. These results highlight the important role played by TEOS/PVP NFs and CNT-TEOS/PVP NFs in improving the compressive strength and toughness of the cement pastes. Observations in previous studies about the nylon 66 nanofibers-modified cementitious materials did not show the efficiency of nanofibers from this perspective [11,12] (see Table 6). Above all, our findings from the mechanical strength tests show a better performance in compressive strength than in tensile strength when introducing TEOS/PVP NFs and CNT-TEOS/PVP NFs into cementitious materials.

Table 6. Effectiveness of TEOS/PVP NFs, CNT-TEOS/PVP NFs, N66 NFs, and CNT-N66 NFs on mechanical properties of cement pastes (increase in % compared with parameters of control samples).

	Previous Works [11,12]				Present Work	
	N66 NFs MCP (1)	N66 NFs MCP (2)	SWCNT-N66 NFs MCP	MWCNT-N66 NFs MCP	T28S/C28S	T28CS/C28CS
CNTs content (wt% in the cement-based materials)	0	0	0.015	0.015	0	0.02
Tensile strength (MPa)	32	28	43	57	6	10
Compressive strength (MPa)	6	8	10	14	28	38
Toughness (J/m ³)	42	49	30	12	54	66

Note: N66 NFs MCP (1): nylon 66 nanofibers-blended cement paste (formic acid–dichloromethane solvent). N66 NFs MCP (2): nylon 66 nanofibers-blended cement paste (formic acid–chloroform solvent). SWCNT-N66 NFs MCP: hybrid nanofibers (single-walled carbon nanotube and nylon 66)-blended cement paste. MWCNT-N66 NFs MCP: hybrid nanofibers (multi-walled carbon nanotube and nylon 66)-blended cement paste.

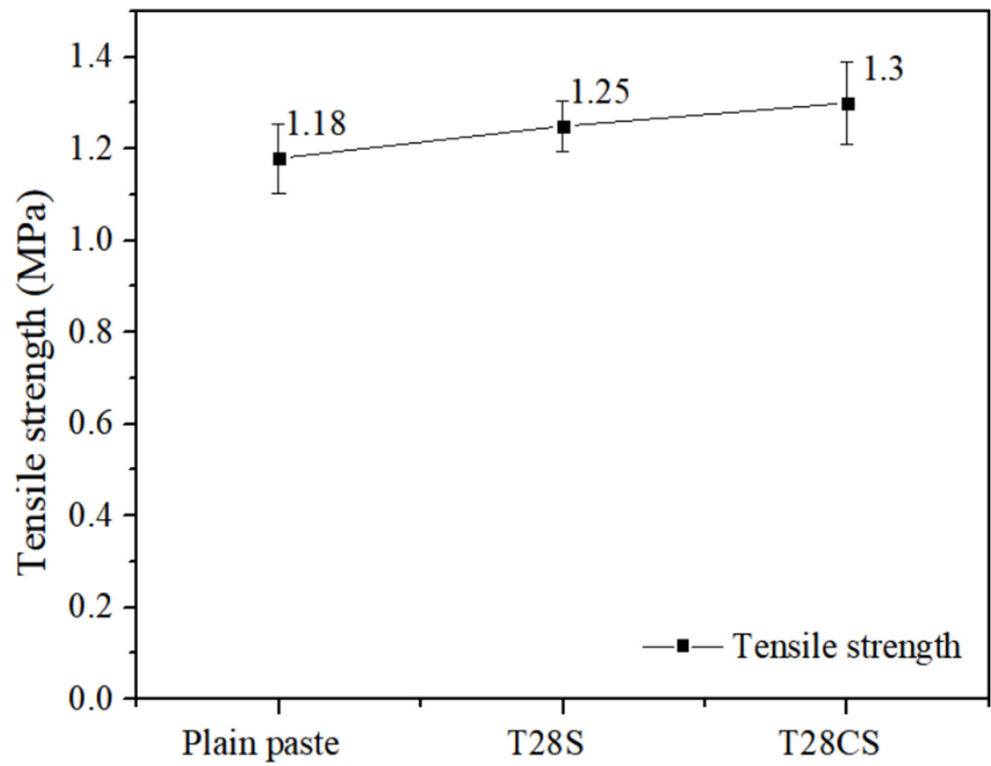


Figure 3. Results from tensile strength test.

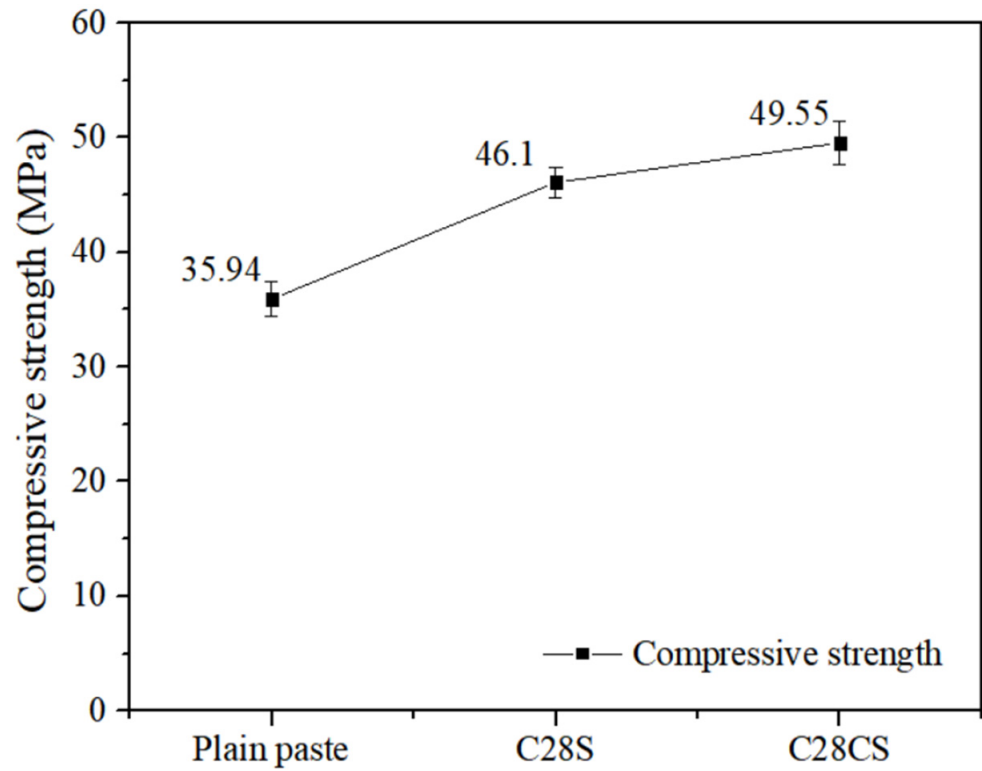


Figure 4. Results from compressive strength test.

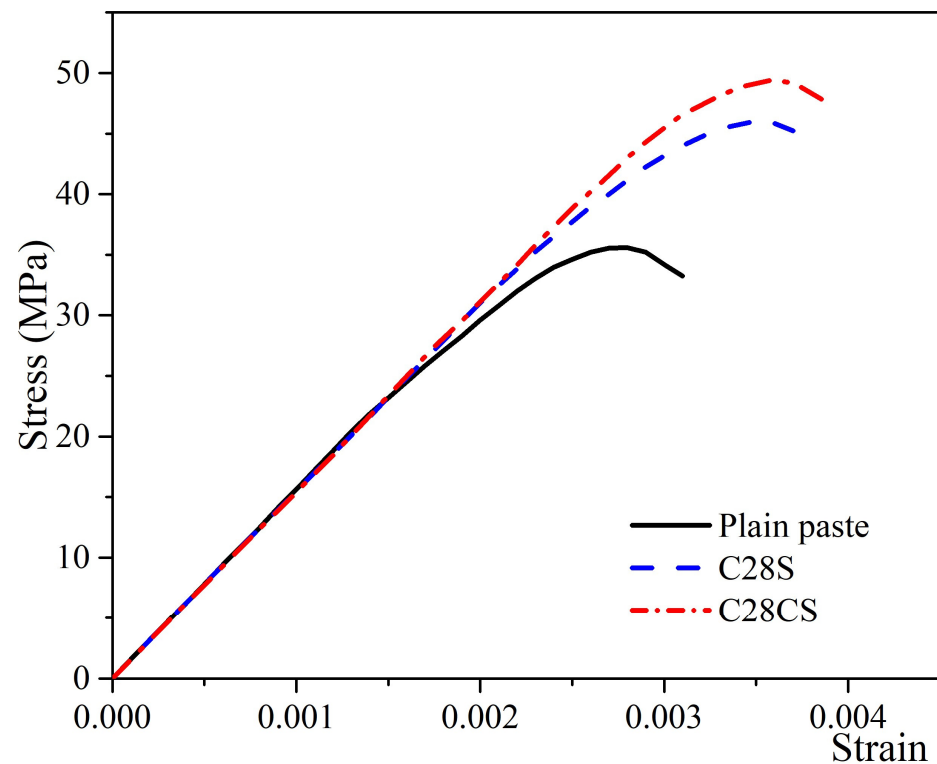


Figure 5. Constitutive curves of hardened plain and modified cement pastes.

Table 7. The 28-day toughness (J/m^3).

	Toughness (J/m^3)
Plain paste	67,898.5
T28S/C28S	104,537.7
T28CS/C28CS	112,933.9

3.2. Morphological Characteristics of Nanofibers

Figure 6 depicts the morphologies of TEOS/PVP NFs and CNT-TEOS/PVP NFs in our study. In general, the electrospun nanofibers tend to overlap each other, forming net layers as a result. Figure 6 shows that the morphologies of both nanofibers are rough and lumpy. This surface texture is desirable when incorporating these nanofibers into cement paste due to the numerous connecting points between the surface of the nanofibers and the cement hydration products. We estimated the mean diameters at 179 nm and 180 nm for TEOS/PVP NFs and CNT-TEOS/PVP NFs, respectively. From the TEM result shown in Figure 7, we determined that CNT-TEOS/PVP NFs and TEOS/PVP NFs are hollow structures (see Figure 7a), which can explain the unimpressive tensile strength results of the proposed fibers in blended cement materials. Figure 7b shows numerous CNTs inside the nanofiber. These CNTs strengthened the nanofibers, leading to slightly better tensile strength results for pastes blended with CNT-TEOS/PVP NFs compared with those blended with TEOS/PVP NFs.

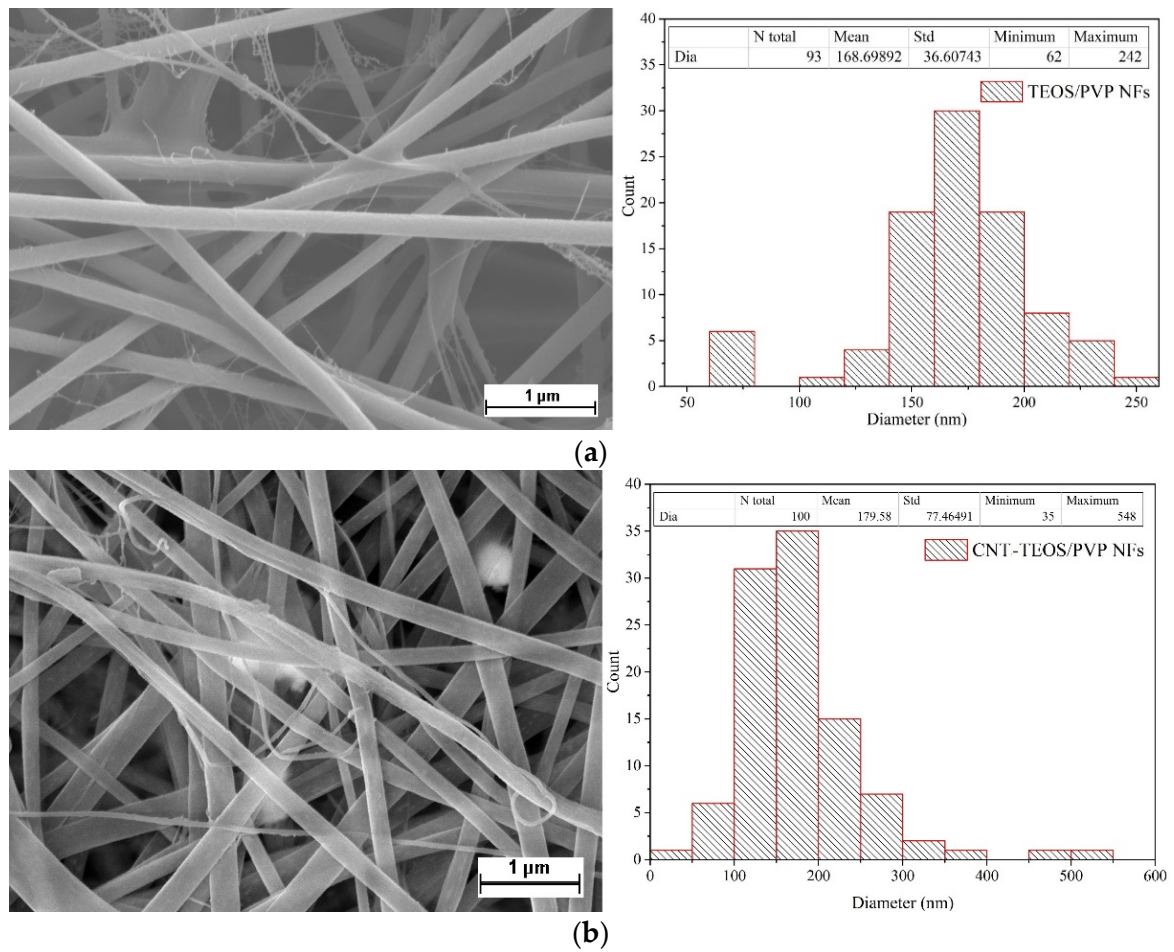


Figure 6. SEM image of nanofibers: (a) TEOS/PVP NFs; (b) CNT-TEOS/PVP NFs.

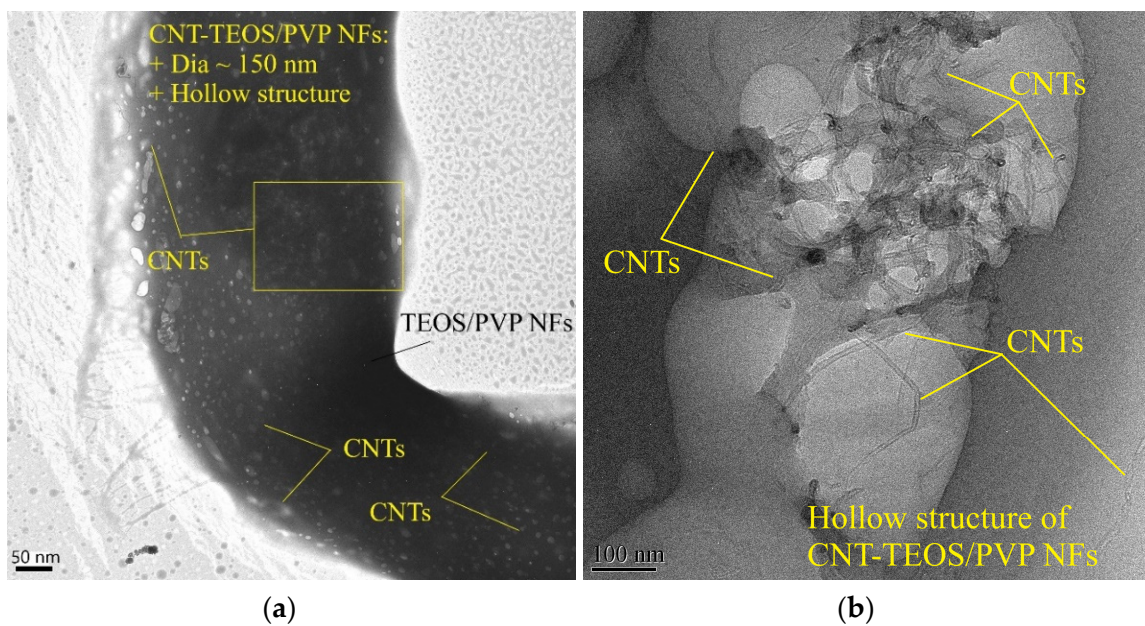


Figure 7. TEM image of CNT-TEOS/PVP NFs: (a) hollow structure of CNT-TEOS/PVP NFs and TEOS/PVP NFs; (b) presence of CNTs inside hybrid nanofibers.

3.3. Microstructure of Hardened Cement Pastes

Figures 8 and 9 present the microstructure of the hardened cement pastes blended with TEOS/PVP NFs and CNT-TEOS/PVP NFs. In both cases, the fibers were interleaved among the hydrates, showing their bridging effect inside the cement matrix. We also found the bridging effect of nanofibers inside the cement matrix's microstructure by using the same method to incorporate nanofibers into cementitious materials [11,12]. Therefore, our proposed method had previously proved its effectiveness in incorporating the electrospun nanofibers into cementitious materials. In our work, despite the bridging effect observed in the cement matrix, the tensile strength of these pastes increased slightly due to the low strength of the electrospun nanofibers, as presented in the previous section. However, these nanofibers made the cement matrix's microstructure more compact because of cross-linking among the cement hydrates, such as calcium silicate hydrates (CHS), calcium hydroxide (CH), ettringite, etc. In addition, the more silicate content added through the nanofibers, the more the CSH content increased. Furthermore, Figures 8b and 9b show that the nanofibers grow out from the cement hydration products, demonstrating the well linking between nanofibers and cement hydrates. As a result, we found a higher compressive strength in the modified cement pastes compared with the plain pastes.

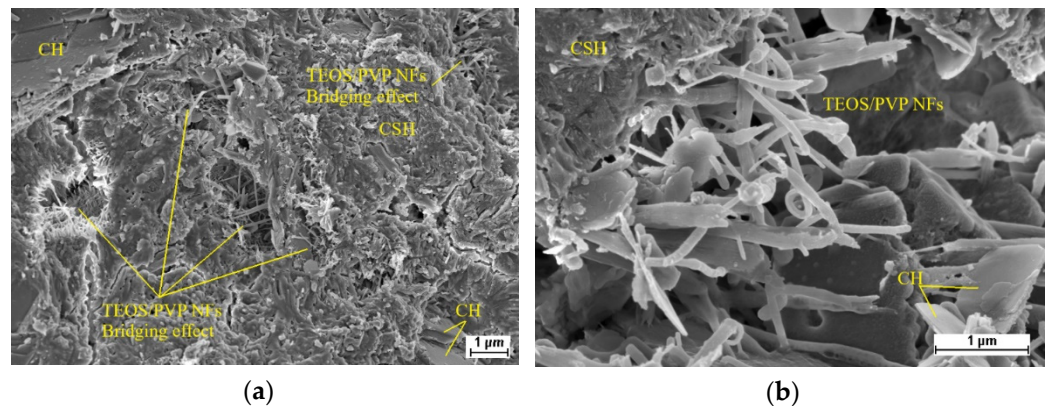


Figure 8. SEM images of cement matrix containing TEOS/PVP NFs. (a) magnification of 20 k, (b) magnification of 50 k.

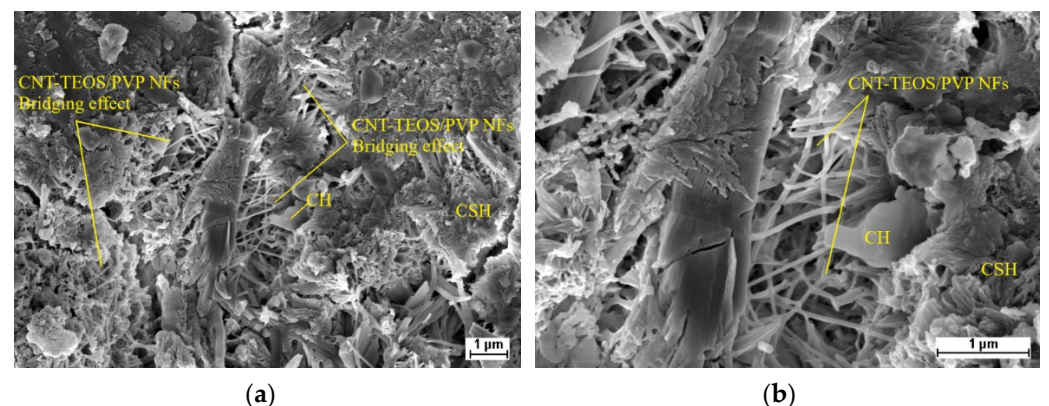


Figure 9. SEM images of cement matrix containing CNT-TEOS/PVP NFs. (a) magnification of 20 k, (b) magnification of 50 k.

3.4. EDS Analysis

Figures 10–14 illustrate our EDS analyses of the surface of the hardened plain cement paste, the hardened cement pastes blended with TEOS/PVP NFs and CNT-TEOS/PVP NFs, and the local zone containing the nanofibers inside the pastes. In general, the element components in all the pastes are consistent together. The main elements of all three samples

are Ca, Si, Al, and O, which are the components of common hydrated products, such as CH, CSH, calcium aluminate hydrates (CAH), etc. [36–40]. The main reactions of the hydration process are shown in Equations (1)–(3) below:



However, the proportion of Si element (in SiO₂) in the plain paste is less than that in the pastes including nanofibers, around 3.57 wt% in the plain paste compared with 4.07 wt% in both pastes blended with TEOS/PVP NFs and CNT-TEOS/PVP NFs (see Figures 10, 11 and 13, and Table 8). Especially in the local zone that contains nanofibers, the proportions of Si element are the highest at around 5.64 wt% and 5.38 wt% in the zone containing TEOS/PVP NFs and CNT-TEOS/PVP NFs, respectively (see Figures 12 and 14, and Table 8). From our results, we observed that the hydration products in all samples are consistent with each other. However, the content of the Si element changed among the three samples. As a result, the more content of the Si element added, the more the CSH component increases. Therefore, the structure becomes more compacted, increasing the material's compressive behavior. Furthermore, a comparison of the ratio between Ca and Si (Ca/Si) can reflect the situation of CSH in cement hydration products. Table 8 shows that the highest Ca/Si ratio belongs to the hardened plain cement paste (4.87), and it reduces in the TEOS/PVP NFs-blended cement paste and the CNT-TEOS/PVP NFs-blended cement paste (3.81 and 2.68, respectively). Singh et al. [41] and Da Silva Andrade et al. [42] concluded that the reduction in the Ca/Si ratio complied with the increase in the silica reactive for the formation of CSH. Therefore, the lowest Ca/Si ratio observed from the EDS analysis of the paste blended with CNT-TEOS/PVP NFs is comparable to the highest previously observed compressive behavior.

Table 8. Elemental analysis from EDS results.

	Element	Wt%	Wt% Sigma	Atomic %	Standard Label
Plain paste	C	6.70	0.41	11.69	C Vit
	O	47.48	0.33	62.21	SiO ₂
	Mg	1.90	0.05	1.64	MgO
	Al	2.17	0.05	1.69	Al ₂ O ₃
	Si	4.78	0.07	3.57	SiO ₂
	S	0.82	0.04	0.54	FeS ₂
	K	1.23	0.05	0.66	KBr
	Ca	33.19	0.24	17.36	Wollastonite
	Fe	1.73	0.11	0.65	Fe
T28S/C28S	C	9.54	0.39	16.40	C Vit
	O	45.00	0.32	58.08	SiO ₂
	Na	0.92	0.05	0.83	Albite
	Mg	0.55	0.04	0.47	MgO
	Al	1.60	0.05	1.22	Al ₂ O ₃
	Si	5.54	0.07	4.07	SiO ₂
	S	0.76	0.04	0.49	FeS ₂
	K	4.46	0.07	2.36	KBr
	Ca	30.14	0.22	15.53	Wollastonite
Fe	1.47	0.11	0.54	Fe	

Table 8. Cont.

	Element	Wt%	Wt% Sigma	Atomic %	Standard Label
T28S/C28S–nanofibers spectrum	C	8.70	0.43	15.06	C Vit
	O	43.63	0.33	56.67	SiO ₂
	Na	1.10	0.05	0.99	Albite
	Mg	3.09	0.06	2.64	MgO
	Al	1.44	0.05	1.11	Al ₂ O ₃
	Si	7.62	0.09	5.64	SiO ₂
	S	0.92	0.05	0.60	FeS ₂
	K	5.05	0.08	2.68	KBr
	Ca	27.44	0.22	14.23	Wollastonite
	Fe	1.01	0.11	0.38	Fe
T28CS/C28CS	C	12.78	0.42	20.49	C Vit
	O	49.00	0.33	58.98	SiO ₂
	Na	1.00	0.05	0.84	Albite
	Mg	0.62	0.04	0.49	MgO
	Al	1.64	0.04	1.17	Al ₂ O ₃
	Si	5.94	0.07	4.07	SiO ₂
	S	0.81	0.04	0.49	FeS ₂
	K	4.34	0.07	2.14	KBr
	Ca	22.75	0.18	10.93	Wollastonite
	Fe	1.14	0.09	0.39	Fe
T28CS/C28CS–nanofibers spectrum	C	8.92	0.41	16.42	C Vit
	O	37.01	0.34	51.15	SiO ₂
	Na	1.19	0.05	1.14	Albite
	Al	1.58	0.05	1.29	Al ₂ O ₃
	Si	6.83	0.08	5.38	SiO ₂
	S	1.44	0.05	0.99	FeS ₂
	K	8.22	0.11	4.65	KBr
	Ca	33.30	0.25	18.37	Wollastonite
		Fe	1.51	0.12	0.60

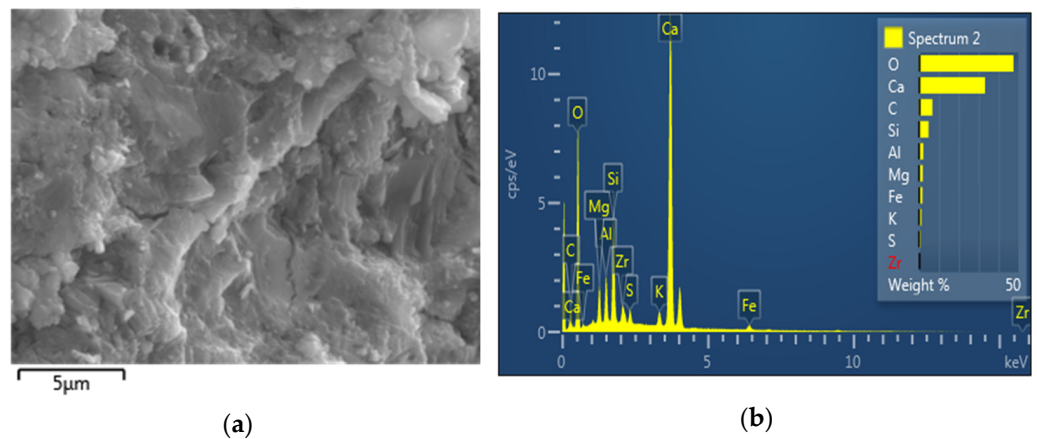


Figure 10. EDS results of plain paste: (a) SEM image; (b) EDS spectrum.

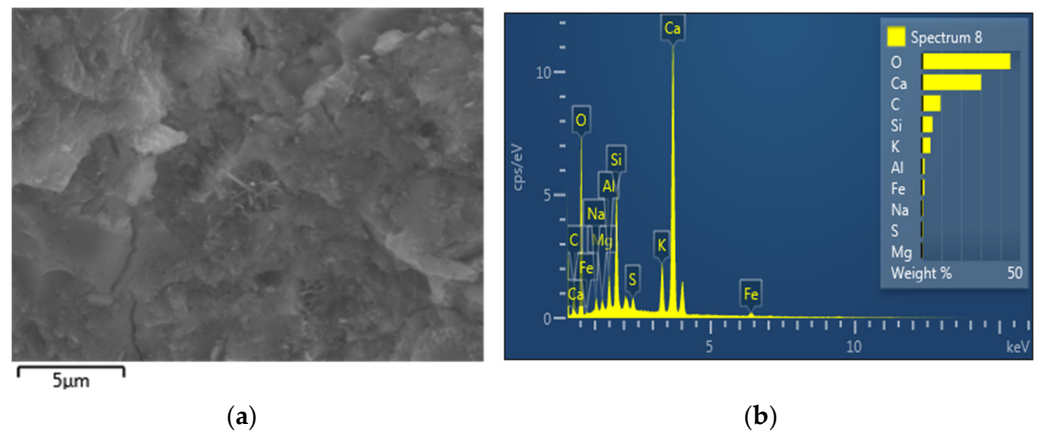


Figure 11. EDS results of cement paste containing TEOS/PVP NFs: (a) SEM image; (b) EDS spectrum.

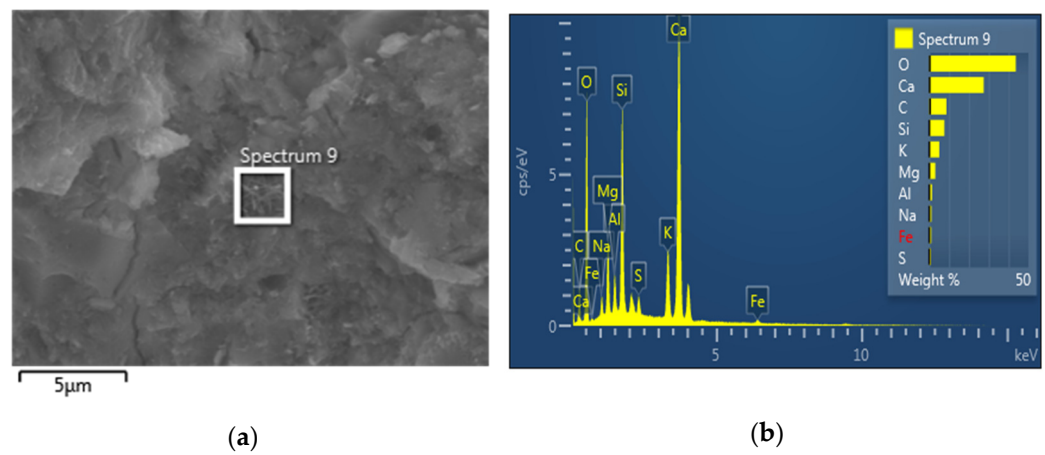


Figure 12. EDS results of cement paste containing TEOS/PVP NFs: (a) SEM image; (b) EDS spectrum—focus on nanofibers zone.

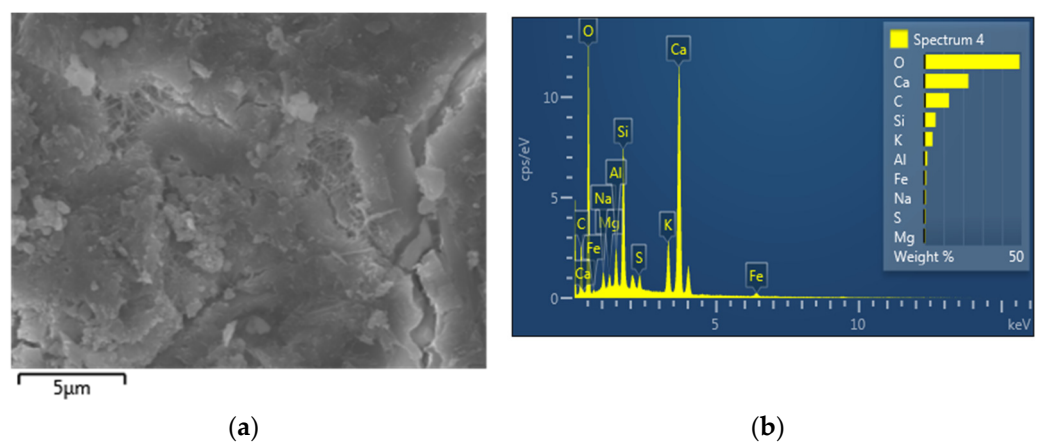


Figure 13. EDS results of cement paste containing CNT-TEOS/PVP NFs: (a) SEM image; (b) EDS spectrum.

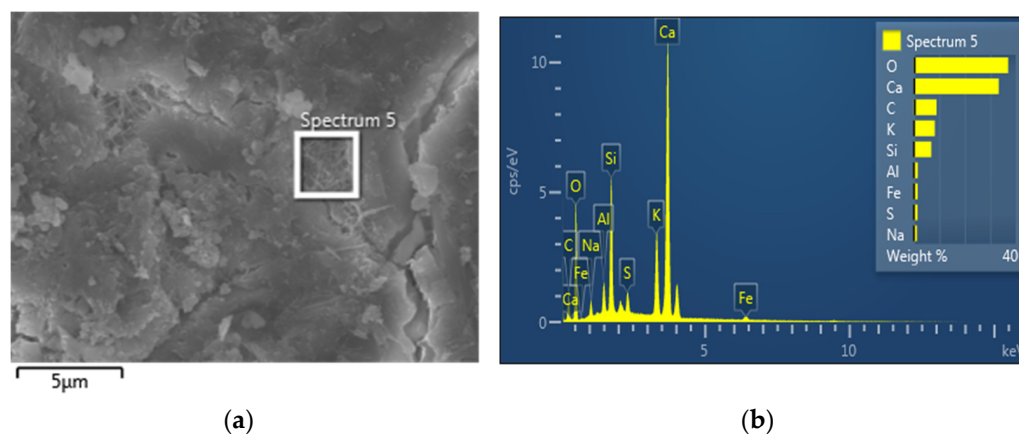


Figure 14. EDS results of cement paste containing CNT-TEOS/PVP NFs: (a) SEM image; (b) EDS spectrum—focus on nanofibers zone.

3.5. Thermal Analysis

Figures 15–18 show the results from thermogravimetric analyses of the modified cement pastes and plain cement paste. Generally, the TGA results show the common curves for hardened cement paste. In the TGA result of the cement pastes before 145 °C, the weight loss belongs to the free water included in each sample [39]. Therefore, for comparing the TGA results of three pastes, the point 100% weight should be put at 145 °C (see Figure 15). The thermal analysis result of the hardened cement paste sample normally consists of three processes, namely the dehydration of CSH, dehydration of CH, and decarbonation of calcite, which are related to three temperature ranges at 145 °C–200 °C, 400 °C–500 °C, and 550 °C–900 °C, respectively [11,12,43–45]. Figure 15 shows that the weight loss from the thermal analysis of the hardened cement paste blended with CNT-TEOS/PVP NFs is the highest, followed by the hardened cement paste blended with TEOS/PVP NFs, while the lowest weight loss belonged to that of the plain paste. Figures 16–18 present the TGA/DTG results of each sample and the detail of the %weight loss that peaked out from the curves. The %weight loss of hydration products from the modified cement pastes is more than that of the plain pastes. Specifically, the amount of CSH phase in the pastes containing TEOS/PVP NFs and CNT-TEOS/PVP NFs is higher than that in the plain pastes. Our findings confirmed that the more compacted structure that developed inside the modified pastes was a result of the increased CSH content. Additionally, CSH is the primary component that formed the long-term strength and durability of cement-based materials [46], explaining the increase in compressive strength. In Figure 18, a peak around 550 °C to 650 °C is attributed to the weight loss of CNTs, which is found in [47]. Above all, the TGA results are suitable with the above results, namely that the higher proportion of hydrates in the cement matrix, which were blended with TEOS/PVP NFs and CNT-TEOS/PVP NFs, explained the increase in the compressive strength of cementitious materials.

Figures 15–18 show the results from thermogravimetric analyses of the modified cement pastes and the plain cement paste. Generally, the TGA results show the common curves for hardened cement paste. As the authors' knowledge, in the TGA result of cement pastes, before 145 °C, the weight loss belongs to the free water included in each sample [39]. Therefore, for comparing the TGA results of three pastes, the point 100% weight should be put at 145 °C (see Figure 15). As reported from the literature, the thermal analysis result of hardened cement paste sample normally consists of three processes the dehydration of CSH, dehydration of CH, and the decarbonation of calcite, which is related to three temperature ranges at 145 °C–200 °C, 400 °C–500 °C, and 550 °C–900 °C, respectively [11,12,43–45]. As can be seen from Figure 15, the weight loss from the thermal analysis of the hardened cement paste blended with CNT-TEOS/PVP NFs is the highest, followed by the observation of the hardened cement paste blended with TEOS/PVP NFs and the lowest weight loss has belonged to that of the plain paste. Figures 16–18 present the TGA/DTG results of each

sample and the detail of %weight loss that peaked out from the curves. It is clear that the %weight loss of hydration products from the modified cement pastes is more than that of the plain pastes. Especially the amount of CSH phase in the pastes containing TEOS/PVP NFs and CNT-TEOS/PVP NFs is higher than that in the plain pastes. These findings confirmed the more compacted structure that developed inside the modified pastes as a result of the increased CSH content. Additionally, CSH is the primary component that forms the long-term strength and durability of cement-based materials [46]. Therefore, the rise in compressive strength can be explained by these observations. In Figure 18, a peak around 550 °C to 650 °C is attributed to the weight loss of CNTs, which is found in [47]. Above all, the TGA results are suitable with the above results. The higher proportion of hydrates in the cement matrix, which were blended with TEOS/PVP NFs and CNT-TEOS/PVP NFs, has been observed and explained for the increase in compressive strength of this cementitious material.

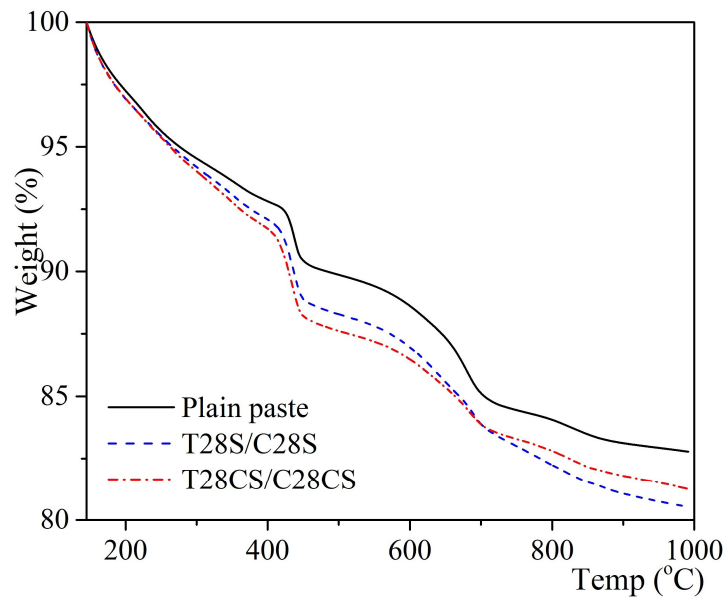


Figure 15. TGA results comparison of three samples.

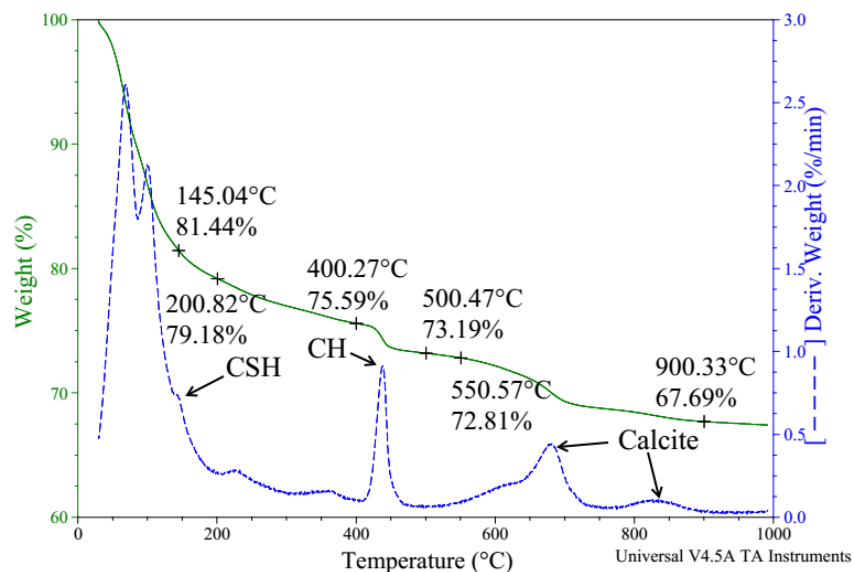


Figure 16. TGA/DTG observations of plain cement paste.

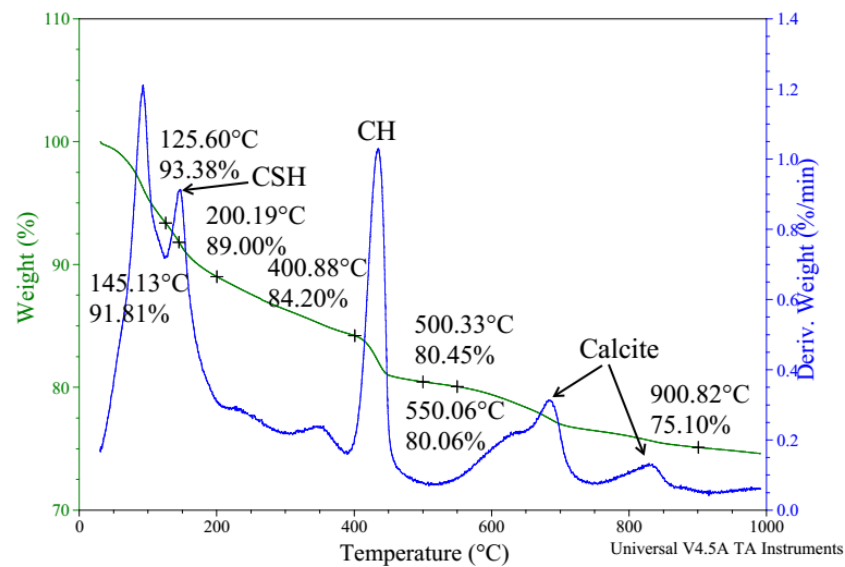


Figure 17. TGA/DTG observations of TEOS/PVP NFs-blended cement paste.

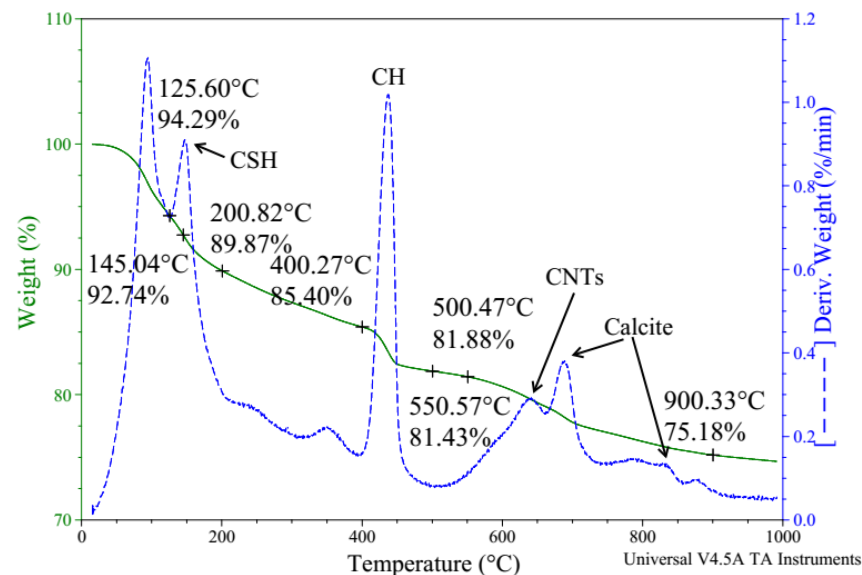


Figure 18. TGA/DTG observations of CNT-TEOS/PVP NFs-blended cement paste.

4. Conclusions

In our study, we showed that tetraethoxysilane/polyvidone nanofibers (TEOS/PVP NFs) and their modified version with carbon nanotubes (CNT-TEOS/PVP NFs) have an impact on the mechanical and microstructural characteristics of cementitious materials. We make the following conclusions considering our findings:

- According to results from mechanical strength testing, adding TEOS/PVP NFs and CNT-TEOS/PVP NFs to cementitious materials results in an increase in compressive strength of 28% and 38% and in toughness characteristics of 54% and 66%, respectively;
- We observed our proposed nanofibers' morphology using SEM and TEM studies. We discovered that TEOS/PVP NFs had a hollow structure by examining TEM images. Additionally, the existence of CNTs was clear;
- We discovered the bridging effect of fibers inside the matrix through SEM images. Additionally, through our EDS and TGA observations, we assessed the change in cement hydrates' proportions and the more compacted structures of the modified cement pastes. Based on these microstructure observations, we showed that a higher percent-

age of cement hydrates combined with the more compacted structure is commensurate with, the higher compressive strength of our survey's samples.

Above all, we regarded the process of adding electrospun nanofibers to the pastes as a useful strategy for strengthening cementitious materials. Our findings can be considered a foundation for increasing cement quality while lowering overall usage, thereby minimizing its environmental impacts. However, more studies are required to optimize the performance of the composite cement manufacturing process and determine the impact of these nanofibers on the other qualities of cement paste and concrete to put this product to use in practical applications.

Author Contributions: Conceptualization, J.J.K.; methodology, T.H.H. and J.J.K.; software, T.N.M.N. and J.K.P.; validation, T.H.H. and J.K.P.; formal analysis, T.N.M.N. and J.K.P.; investigation, T.H.H. and J.J.K.; data curation, J.J.K. and T.N.M.N.; writing—original draft preparation, T.N.M.N. and J.K.P.; writing—review and editing, T.N.M.N., J.K.P., T.H.H. and J.J.K.; visualization, T.H.H.; supervision, J.J.K.; project administration, T.H.H.; funding acquisition, T.H.H. All authors have read and agreed to the published version of the manuscript.

Funding: This research was supported by the Korea Institute of Marine Science & Technology Promotion (KIMST), funded by the Ministry of Oceans and Fisheries (20220364).

Institutional Review Board Statement: Not applicable.

Informed Consent Statement: Not applicable.

Data Availability Statement: Not applicable.

Conflicts of Interest: The authors declare no conflict of interest.

References

1. Hamada, H.M.; Al-Attar, A.; Shi, J.; Yahaya, F.; Al Jawahery, M.S.; Yousif, S.T. Optimization of sustainable concrete characteristics incorporating palm oil clinker and nano-palm oil fuel ash using response surface methodology. *Powder Technol.* **2023**, *413*, 118054. [[CrossRef](#)]
2. Zhang, M.; Zhu, X.; Liu, B.; Shi, J.; Gencel, O.; Ozbakkaloglu, T. Mechanical property and durability of engineered cementitious composites (ECC) with nano-material and superabsorbent polymers. *Powder Technol.* **2022**, *409*, 117839. [[CrossRef](#)]
3. Wang, H.; Shen, J.; Liu, J.; Lu, S.; He, G. Influence of carbon nanofiber content and sodium chloride solution on the stability of resistance and the following self-sensing performance of carbon nanofiber cement paste. *Case Stud. Constr. Mater.* **2019**, *11*, e00247. [[CrossRef](#)]
4. Wang, H.; Gao, X.; Wang, R. The influence of rheological parameters of cement paste on the dispersion of carbon nanofibers and self-sensing performance. *Constr. Build. Mater.* **2017**, *134*, 673–683. [[CrossRef](#)]
5. Saleh, H.M.; El-Sheikh, S.M.; Elshereafy, E.E.; Essa, A.K. Performance of cement-slag-titanate nanofibers composite immobilized radioactive waste solution through frost and flooding events. *Constr. Build. Mater.* **2019**, *223*, 221–232. [[CrossRef](#)]
6. Saleh, H.M.; El-Sheikh, S.M.; Elshereafy, E.E.; Essa, A.K. Mechanical and physical characterization of cement reinforced by iron slag and titanate nanofibers to produce advanced containment for radioactive waste. *Constr. Build. Mater.* **2019**, *200*, 135–145. [[CrossRef](#)]
7. Chinchillas-Chinchillas, M.J.; Gaxiola, A.; Alvarado-Beltrán, C.G.; Orozco-Carmona, V.M.; Pellegrini-Cervantes, M.J.; Rodríguez-Rodríguez, M.; Castro-Beltrán, A. A new application of recycled-PET/PAN composite nanofibers to cement-based materials. *J. Clean. Prod.* **2020**, *252*, 119827. [[CrossRef](#)]
8. McElroy, P.; Emadi, H.; Surowiec, K.; Casadonte, D.J. Mechanical, rheological, and stability performance of simulated in-situ cured oil well cement slurries reinforced with alumina nanofibers. *J. Pet. Sci. Eng.* **2019**, *183*, 106415. [[CrossRef](#)]
9. de Azevedo, N.H.; Gleize, P.J.P. Effect of silicon carbide nanowhiskers on hydration and mechanical properties of a Portland cement paste. *Constr. Build. Mater.* **2018**, *169*, 388–395. [[CrossRef](#)]
10. Abu Al-Rub, R.; Tyson, B.M.; Yazdanbakhsh, A.; Grasley, Z. Mechanical Properties of Nanocomposite Cement Incorporating Surface-Treated and Untreated Carbon Nanotubes and Carbon Nanofibers. *J. Nanomech. Micromech.* **2012**, *2*. [[CrossRef](#)]
11. Nguyen, T.N.M.; Yoo, D.-Y.; Kim, J.J. Cementitious material reinforced by carbon nanotube-Nylon 66 hybrid nanofibers: Mechanical strength and microstructure analysis. *Mater. Today Commun.* **2020**, *23*, 100845. [[CrossRef](#)]
12. Nguyen, T.N.M.; Moon, J.; Kim, J.J. Microstructure and mechanical properties of hardened cement paste including Nylon 66 nanofibers. *Constr. Build. Mater.* **2020**, *232*, 117134. [[CrossRef](#)]
13. Kim, J.J.; Nguyen, T.N.M.; Nguyen, X.T.; Ta, D.H. Reinforcing cementitious material using single-walled carbon nanotube—nylon 66 nanofibers. *Transp. Commun. Sci. J.* **2020**, *71*, 46–55. [[CrossRef](#)]

14. Thenmozhi, S.; Dharmaraj, N.; Kadirvelu, K.; Kim, H.Y. Electrospun nanofibers: New generation materials for advanced applications. *Mater. Sci. Eng. B* **2017**, *217*, 36–48. [[CrossRef](#)]
15. Xue, J.; Xie, J.; Liu, W.; Xia, Y. Electrospun Nanofibers: New Concepts, Materials, and Applications. *Acc. Chem. Res.* **2017**, *50*, 1976–1987. [[CrossRef](#)] [[PubMed](#)]
16. Arinstein, A. *Electrospun Polymer Nanofibers, chapter 1*; Pan Stanford Publishing Pte. Ltd.: Stanford, CA, USA, 2018; pp. 1–4.
17. Patel, A.C.; Li, S.; Wang, C.; Zhang, W.; Wei, Y. Electrospinning of Porous Silica Nanofibers Containing Silver Nanoparticles for Catalytic Applications. *Chem. Mater.* **2007**, *19*, 1231–1238. [[CrossRef](#)]
18. Tsou, P.-H.; Chou, C.-K.; Saldana, S.M.; Hung, M.-C.; Kameoka, J. The fabrication and testing of electrospun silica nanofiber membranes for the detection of proteins. *Nanotechnology* **2008**, *19*, 445714. [[CrossRef](#)]
19. Veverková, I.; Lovětinská-Šlamborová, I. Modified Silica Nanofibers with Antibacterial Activity. *J. Nanomater.* **2016**, *2016*, 2837197. [[CrossRef](#)]
20. Henry, N.; Clouet, J.; Le Visage, C.; Weiss, P.; Gautron, E.; Renard, D.; Cordonnier, T.; Boury, F.; Humbert, B.; Terrisse, H.; et al. Silica nanofibers as a new drug delivery system: A study of the protein–silica interactions. *J. Mater. Chem. B* **2017**, *5*, 2908–2920. [[CrossRef](#)]
21. Tepekiran, B.N.; Calisir, M.D.; Polat, Y.; Akgul, Y.; Kilic, A. Centrifugally spun silica (SiO₂) nanofibers for high-temperature air filtration. *Aerosol Sci. Technol.* **2019**, *53*, 921–932. [[CrossRef](#)]
22. Choi, S.-S.; Lee, S.G.; Im, S.S.; Kim, S.H.; Joo, Y.L. Silica nanofibers from electrospinning/sol-gel process. *J. Mater. Sci. Lett.* **2003**, *22*, 891–893. [[CrossRef](#)]
23. Newsome, T.E.; Olesik, S.V. Silica-based nanofibers for electrospun ultra-thin layer chromatography. *J. Chromatogr. A* **2014**, *1364*, 261–270. [[CrossRef](#)] [[PubMed](#)]
24. Freyer, A.; Savage, N.O. Effects of Sol Viscosity and Application to Thin Layer Chromatography. In *The Science and Function of Nanomaterials: From Synthesis to Application*; American Chemical Society: New York, NY, USA, 2014. [[CrossRef](#)]
25. Shahhosseininia, M.; Bazgir, S.; Joupari, M.D. Fabrication and investigation of silica nanofibers via electrospinning. *Mater. Sci. Eng. C* **2018**, *91*, 502–511. [[CrossRef](#)] [[PubMed](#)]
26. Cheng, Q.; Debnath, S.; Gregan, E.; Byrne, H.J. Ultrasound-Assisted SWNTs Dispersion: Effects of Sonication Parameters and Solvent Properties. *J. Phys. Chem. C* **2010**, *114*, 8821–8827. [[CrossRef](#)]
27. Huang, Y.Y.; Terentjev, E.M. Dispersion of Carbon Nanotubes: Mixing, Sonication, Stabilization, and Composite Properties. *Polymers* **2012**, *4*, 275–295. [[CrossRef](#)]
28. Yang, K.; Yi, Z.; Jing, Q.; Yue, R.; Jiang, W.; Lin, D. Sonication-assisted dispersion of carbon nanotubes in aqueous solutions of the anionic surfactant SDBS: The role of sonication energy. *Chin. Sci. Bull.* **2013**, *58*, 2082–2090. [[CrossRef](#)]
29. Sabet, S.M.; Mahfuz, H.; Hashemi, J.; Nezakat, M.; Szpunar, J.A. Effects of sonication energy on the dispersion of carbon nanotubes in a vinyl ester matrix and associated thermo-mechanical properties. *J. Mater. Sci.* **2015**, *50*, 4729–4740. [[CrossRef](#)]
30. *ASTM C150*; Standard Specification for Portland Cement. ASTM International: West Conshohocken, PA, USA, 2020.
31. Rao, A.M.; Chen, J.; Richter, E.; Schlecht, U.; Eklund, P.C.; Haddon, R.; Venkateswaran, U.D.; Kwon, Y.-K.; Tomanek, D. Effect of van der Waals Interactions on the Raman Modes in Single Walled Carbon Nanotubes. *Phys. Rev. Lett.* **2001**, *86*, 3895–3898. [[CrossRef](#)]
32. Sabba, Y.; Thomas, E.L. High-Concentration Dispersion of Single-Wall Carbon Nanotubes. *Macromolecules* **2004**, *37*, 4815–4820. [[CrossRef](#)]
33. Che, J.; Wu, K.; Lin, Y.; Wang, K.; Fu, Q. Largely improved thermal conductivity of HDPE/expanded graphite/carbon nanotubes ternary composites via filler network-network synergy. *Compos. Part A Appl. Sci. Manuf.* **2017**, *99*, 32–40. [[CrossRef](#)]
34. *ASTM C307*; Standard Test Method for Tensile Strength of Chemical-Resistant Mortar, Grouts, and Monolithic Surfacing. ASTM International: West Conshohocken, PA, USA, 2018.
35. *ASTM C109*; Standard Test Method for Compressive Strength of Hydraulic Cement Mortars (Using 2-in. or [50 mm] Cube Specimens). ASTM International: West Conshohocken, PA, USA, 2020.
36. Mohammed, S.; Elhem, G.; Mekki, B. Valorization of pozzolanicity of Algerian clay: Optimization of the heat treatment and mechanical characteristics of the involved cement mortars. *Appl. Clay Sci.* **2016**, *132–133*, 711–721. [[CrossRef](#)]
37. Neville, A.M. *Properties of Concrete*, 5th ed.; Pearson, Prentice Hall: London, UK, 2005.
38. Vedalakshmi, R.; Raj, A.S.; Srinivasan, S.; Babu, K.G. Quantification of hydrated cement products of blended cements in low and medium strength concrete using TG and DTA technique. *Thermochim. Acta* **2003**, *407*, 49–60. [[CrossRef](#)]
39. Taylor, H.F.W. *Cement Chemistry*; Thomas Telford: London, UK, 1997; Chapter 5.
40. Mehta, P.K.; Monteiro, P.J.M. *Concrete: Microstructure, Properties, and Materials*; The McGraw-Hill Companies, Inc: New York, NY, USA, 2006; Chapter 6; pp. 203–252. [[CrossRef](#)]
41. Singh, L.; Zhu, W.; Howind, T.; Sharma, U. Quantification and characterization of C-S-H in silica nanoparticles incorporated cementitious system. *Cem. Concr. Compos.* **2017**, *79*, 106–116. [[CrossRef](#)]
42. Andrade, D.D.S.; Rêgo, J.H.D.S.; Morais, P.C.; Lopes, A.N.D.M.; Rojas, M.F. Investigation of C-S-H in ternary cement pastes containing nanosilica and highly-reactive supplementary cementitious materials (SCMs): Microstructure and strength. *Constr. Build. Mater.* **2019**, *198*, 445–455. [[CrossRef](#)]
43. Kim, J.J.; Foley, E.M.; Taha, M.M.R. Nano-mechanical characterization of synthetic calcium–silicate–hydrate (C–S–H) with varying CaO/SiO₂ mixture ratios. *Cem. Concr. Compos.* **2013**, *36*, 65–70. [[CrossRef](#)]

44. Foley, E.M.; Kim, J.J.; Taha, M.M.R. Synthesis and nano-mechanical characterization of calcium-silicate-hydrate (C-S-H) made with 1.5 CaO/SiO₂ mixture. *Cem. Concr. Res.* **2012**, *42*, 1225–1232. [[CrossRef](#)]
45. Wongkeo, W.; Thongsanitgarn, P.; Chindapasirt, P.; Chaipanich, A. Thermogravimetry of ternary cement blends—Effect of different curing methods. *J. Therm. Anal.* **2013**, *113*, 1079–1090. [[CrossRef](#)]
46. Mehta, P.K.; Monteiro, P.J.M. *Concrete: Microstructure, Properties, and Materials*, 4th ed.; McGraw-Hill Education: New York, NY, USA, 2013.
47. Bom, D.; Andrews, R.; Jacques, D.; Anthony, J.; Chen, B.; Meier, M.S.; Selegue, J.P. Thermogravimetric Analysis of the Oxidation of Multiwalled Carbon Nanotubes: Evidence for the Role of Defect Sites in Carbon Nanotube Chemistry. *Nano Lett.* **2002**, *2*, 615–619. [[CrossRef](#)]

Disclaimer/Publisher’s Note: The statements, opinions and data contained in all publications are solely those of the individual author(s) and contributor(s) and not of MDPI and/or the editor(s). MDPI and/or the editor(s) disclaim responsibility for any injury to people or property resulting from any ideas, methods, instructions or products referred to in the content.